

Removal of Hydrogen Poisoning by Electrostatically Polar MgO Support for Low Pressure NH₃ Synthesis at High Rate over Ru Catalyst

Simson Wu^{1†}, Yung-Kang Peng^{1†}, Tian-Yi Chen¹, Jiaying Mo¹, Alex Large⁴, Ian McPherson¹, Hung-Lung Chou², Ian Wilkinson³, Federica Venturini⁵, David Grinter⁵, Pilar Ferrer Escorihuela⁵, Georg Held^{4,5} and Shik Chi Edman Tsang^{1*}

¹Wolfson Catalysis Centre, Department of Chemistry University of Oxford, Oxford, OX1 3QR, UK

²Graduate Institute of Applied Science and Technology, National Taiwan University of Science and Technology, Taipei 10617, Taiwan

³Siemens plc, CT NTF, Wharf Road, Oxford OX29 4BP (UK)

⁴University of Reading, Reading RG6 6UR (UK)

⁵Diamond Light Source, Didcot OX11 0DE (UK)

[†]equal contribution as co-first author; corresponding e-mail: edman.tsang@chem.ox.ac.uk

ABSTRACT: The increasing availability of low-cost and low pressure, renewable H₂ from wind and solar means has triggered tremendous interest in developing low pressure ammonia synthesis with N₂ as energy carrier as well as green fertilizer. As such Cs-promoted Ru/MgO catalysts used in Kellogg process show superiority to Fe-based catalysts at milder conditions, however, as known, the surface poisoning of Ru sites by competitive strong H₂ dissociative adsorption limits the overall rate. It is demonstrated for the first time that the use of simple electrostatically polar MgO(111) to replace non-polar MgO as support can significantly alleviate the hydrogen poisoning and facilitate an unprecedented ammonia production rate by its high intrinsic proton capture ability.

1 Introduction:

Ammonia synthesis is one of the key industrial processes that consumes more than 1% of the power generated globally per year¹, where the majority of the ammonia synthesised is used for the production of nitrogen fertilizers. On the other hand, new opportunities of using ammonia as a hydrogen carrier via water electrolysis from renewable energy sources (solar, wind and tidal means) has attracted a lot of attention due to its high hydrogen density and high round-trip efficiency as e-HB process^{2,3}. Traditionally, ammonia is synthesised *via* large-scale Haber-Bosch process over commercial iron catalysts, which requires high pressure and high temperature (>500 °C and 25 MPa) for the catalyst to work efficiently^{4,5}. The demands for extreme reaction conditions and safe but bulk installation have made the process unfavourable in terms of energy efficiency. Alternatively, ruthenium-based catalysts have a much higher intrinsic activity than iron catalysts and can operate at a lower pressure. Recent advances in harnessing renewable energies have given rise to new possibilities in building smaller-scale reactor unit for ammonia production to couple with the upstream H₂ generation to justify the high cost of ruthenium³. There have been some recent studies to employ new Ru based catalysts at lower temperature^{6,16} in ammonia synthesis although the energy required maintaining the reactor temperature is less critical for this exothermic reaction. The use of higher temperature would also favor faster kinetics provided the catalysts are stable under the high temperature conditions. However, for the development of a small reactor, the

main challenge is how to produce ammonia efficiently at lower pressure with recycling unreacted substrates use dihydrogen at its low production temperature and especially pressure (< 5 MPa) without using expensive pressure ramping and cumbersome high pressure installations, since the generally unfavorable kinetics and the strong thermodynamic barrier of the nitrogen triple bond dissociation (941 kJ/mol) limit ammonia rates under such mild conditions. Thus, hydrogen manufactured from an electrolyser at low pressure would require coupling with a more efficient Ru catalyst to achieve high ammonia production rate in smaller and flexible eHB units for deployment.

Aika *et al.* has performed a systematic study on various metal oxides support for the ruthenium-based catalysts and found that Ru/MgO attained the highest activity compared to CaO, Al₂O₃ and TiO₂⁷. It was also discovered that the catalytic performance can be increased by several orders after the addition of the alkali promoter. After decades of investigations, the Cs-Ru/MgO configuration has been commercially used as one of the best industrial catalytic systems in Kellogg process at relatively low pressure. Most researchers have attributed this to the strong basicity of MgO which renders high charge density of the surface Ru nanoparticle (NP) for back electron donation to activate dinitrogen^{8,9}. However, ruthenium-based catalysts are still easily prone to hydrogen poisoning, especially at relative high hydrogen to nitrogen partial pressures and under mild reaction conditions^{10,11}. It is well-known that typical hydrogen rate order for the synthesis of ammonia over traditional Cs-Ru/MgO catalysts is around -1^{5,8,12}. This means that the disso-

ciative chemisorption of hydrogen precedes that of nitrogen, resulting in partial blockage of Ru active sites by these hydrogen adatoms and eventually preventing effective dissociative chemisorption of N₂. This hydrogen poisoning effect would be amplified by the increase in total pressure, resisting the formation of ammonia at higher rate. Thus, a fast removal of hydrogen from Ru surface is of crucial importance to ensure effective ammonia production.

Given that each facet of a crystallite possesses distinctive intrinsic energy and atomic arrangement, tailoring particle physiochemical properties by exposing a particular facet has recently attracted a significant attention¹³. Herein, a great enhancement in ammonia production of Cs-Ru/MgO was simply achieved by replacing polycrystalline MgO support with electrostatically polar MgO (111) surface (cf. nonpolar (110) and (100) surfaces). The basicity strength of surface [O] and the H⁺ stabilization of polar surface were found to efficiently alleviate hydrogen poisoning to Ru site with a highly positive H₂ rate order (+0.6), and thus render a significant increase in catalytic performance.

2 Results and Discussion:

The syntheses of MgO nanocrystals with preferential exposed (111)¹⁴, (110)¹⁵, and (100)¹⁵ facets have been well-established in literature and denoted as MgO(111), MgO(110) and MgO(100) in this study. MgO(111) was obtained by the calcination of Mg(OH)₂ prepared via the surfactant-assisted hydrothermal process¹⁴. MgO(110) and MgO(100) were prepared by the vacuum calcination of commercial MgO¹⁵ and the thermal decomposition of Mg(NO₃)₂¹⁵, respectively. The transmission electron microscopy (TEM) and high resolution TEM images of MgO(111) in Fig. S1a reveal the majority of sheet-like NPs and lattice fringes with a distance of 0.244 nm parallel to the main surface of the nanosheet, which is in good agreement with the (111) lattice spacing in literature¹⁴. The leaf-like MgO(110) shown in Fig. S1b shows lattice fringes of 0.148 nm, suggesting the main exposed facet is (110)¹⁵. The thermal decomposition of Mg(NO₃)₂ generates MgO(100) with a lattice spacing of 0.214 nm, which corresponds to the (100) plane¹⁵ (Fig. S1c). Also see Fig. S2 for corresponding scanning electron microscopy (SEM) images. XRD analysis (Fig. S3) confirms all MgO samples are typical rock-salt structure and suggests particle size in the order of MgO(100) > MgO(111) > MgO(110). This order can be further supported by the BET measurement (Table S1).

Table 1 shows the comparative catalytic performance ammonia production rate over Cs-Ru/MgO using different MgO facet supports with various recent reported Ru based catalysts in literature. As seen from Table 1, Ru based catalysts generally show good activity under our evaluated conditions of 673 K and 1 MPa at comparable weight hour space velocity at N₂/H₂ of 3:1. It is interesting to find that the activity of Ru metal seems to depend on the nature of support material used. It is exciting to see that the use of polar MgO(111) support gives the best activity per mole of Ru used (93.7 μmol NH₃ Ru-mol⁻¹h⁻¹) as it is critically important to use this expensive metal effectively for the catalysis.

Fig. 1a carefully compares the ammonia production rate of Cs-promoted Ru supported on MgO(111), MgO(110) and MgO(100) under similar reaction conditions and metal loading. Cs-Ru/MgO has been evaluated as the benchmark of catalytic activity and Ru/Pr₂O₃¹⁶ has been recently reported as a novel catalyst due to its active Ru nano-layers. At 673 K and 1.0 MPa, Cs-Ru/MgO(111) displays a stable and record-high activity at 93.7 μmetal-mol g⁻¹ h⁻¹, which is 4.5 times as high as the commercial MgO catalyst whereas Cs-Ru/MgO(100) has an activity comparable to the commercial Kellogg type of catalyst reported in literature (see Table 1). Interestingly, as hydrogen partial pressure increases (when H₂:N₂ = 3.5:1), the difference in activity is becoming more pronounced between

(111) and other facets. Meanwhile, all three supports exhibit similar apparent activation energy (~118 kJ mol⁻¹, Fig. S4a), which is in good agreement with the values for dissociative nitrogen activation reported in literature for typical Cs-Ru/MgO catalyst^{17,18}. This activity order indicates that neither crystallinity nor surface area are the key factors. This is because MgO(110) possessing similar crystallinity as MgO(111) (Fig. S3) but highest surface area among three supports (Table S1) only gives 52% of the activity as the latter, which has less than 33% surface area of MgO(111). The role of defect is also proved to be minor by electron paramagnetic resonance (EPR) as no internal (g~1.98) and surface (g~2.05) defect can be observed for MgO(111) but MgO(100) and MgO(110) support (Fig. S5). The Ru size effect is excluded here as the size distribution of Ru NP is very similar (2 nm) on three MgO supports as evidenced by TEM (Fig. S6). Since the unusual activity of MgO(111) has been attributed to the surface basicity^{14,19}, CO₂-temperature programmed desorption (TPD) was further carried out (Fig. S7). Generally, peaks in the CO₂-TPD suggest basic sites (i.e. oxygen) increasing in strength as the temperature increases: hydroxyl groups (20~160°C) < oxygen in Mg²⁺ and O²⁻ pairs (160~400°C) < low coordinated oxygen anions (>400°C)²⁰. However, no expected difference in CO₂-TPD pattern can be observed among MgO supports, presumably due to the TPD technique is not able to distinguish subtle differences in the distribution of base sites, leading to simple profiles of an averaged base strength²¹. The corresponding overall CO₂ adsorption (mmol/g) and basic site density (mmol-m⁻²) both show the order of MgO(111) > MgO(110) > MgO(100) (Table 1). Even though the order of basic site density derived from CO₂-TPD matches the activity result at this stage, some important questions remain to be answered. First, the nature of basic sites responsible for the observed activity is not yet clear. Secondly, the corresponding mechanism is not known.

Accordingly, kinetic studies of nitrogen and hydrogen with various partial pressures were performed (the kinetic parameters evaluated at differential conditions at low conversions are summarized in Table 2). It is found in Fig. S4b that the reaction order of N₂ for all three MgO supports is almost the same in the rate equation for ammonia synthesis ($r = kP_{N_2}^{\alpha}P_{H_2}^{\beta}P_{NH_3}^{\gamma}$). This indicates that the catalytic activity of using different MgO supports does not have any correlation with the N₂ dissociation, which is regarded as the rate-determining-step for traditional ruthenium catalysts^{8,17,22}. The similar apparent activation energy derived from the Arrhenius plots again shows that the rate determining step (RDS) between the supports is essentially the same (Fig. S4a). Surprisingly, a distinct difference in the H₂ reaction order was found between MgO supports used (Fig. 1b). MgO(100) shows similar H₂ order of -0.5 as reported for all Cs-Ru/MgO catalyst, while MgO(111), for the first time, gives not only positive value but as high as +0.6 at 643K, a temperature known for significant hydrogen poisoning for Ru-based catalysts⁶. Given that a negative H₂ order suggests the poisoning of Ru active sites by dissociated hydrogen adatoms (i.e. preventing effective dissociative chemisorption of N₂ on the competitive Ru sites), a highly positive H₂ order indicates that the hydrogen removal rate on Ru surface is extremely effective and therefore gives higher activity. The hydrogen retardation index as proposed by Aika *et. al.* was also calculated²³. Interestingly, Cs-Ru/MgO(111) is the only catalyst observed so far to display a negative index whereas the retarded species in positive index are dominated by H adatoms and surface NH_x intermediates (Fig. 1c). This is again indicative that the hydrogen poisoning problem is significantly alleviated by the simply using of the polar MgO(111) support surface. A hydrogen rate order study for Ru supported on different dominant facets of MgO was also performed to rule out the contribution of Cs, which again shows a positive hydrogen order for MgO(111) in contrast to

the other 2 facets (Figure S8). CO chemisorption and H chemisorption were also performed accordingly to investigate the nature and extent of the adsorbed H species (Fig. 1d). As expected the difference between CO and H chemisorption for Ru/MgO(100) and Ru/MgO(110) is minimal since both CO and H are adsorbed in the same manner (head-on) on Ru. Interestingly, it shows a stark contrast between the CO and H chemisorption for the Ru/MgO(111), implying that a substantial additional quantity of H is dwelled on the MgO(111) support. A stability test of 100 hours under reaction condition suggests the regenerative nature of such an effect (Fig. S9). The MgO support was replaced by activated carbon (AC) and kept other reaction conditions the same for the kinetic H₂ order study. As shown in Table 2, it is clear that the H₂ poisoning on Cs-Ru/AC has still been observed under relatively high H₂ partial pressure. In stark contrast, the use of MgO with preferential exposed (111) surface can remove the H₂ poisoning on Ru nanoparticle by switching the negative H₂ order to a highly positive value under the same condition.

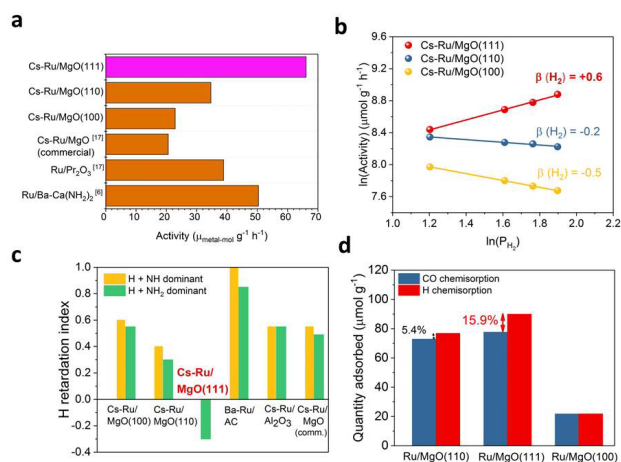


Figure 1. (a) Comparison of ammonia production activity (μmol metal⁻¹ g⁻¹ h⁻¹) normalised by Ru weight% loading at 673 K, 1.0 MPa and moderate WHSV (below 36000 mL g⁻¹ h⁻¹). (b) Dependence of ammonia synthesis rate of Cs-promoted Ru supported on MgO(111), MgO(110), and MgO(100) on H₂ at 643 K and 1.0 MPa. Reaction conditions: catalysts, 0.1 g; synthesis gas, H₂/N₂ = 3 with a flow rate of 60 ml min⁻¹. See SI for details. The error range, defined as the standard deviation for a set of experimental runs, was ±5%. (c) Hydrogen retardation index of the MgO catalysts compared to other reported system. Values of AC, Al₂O₃ and commercial polycrystalline MgO were extracted from the literature by Aika *et al.*²³. (d) Chemisorption measurements on CO and H₂ of the Ru on MgO catalysts. The quantification of adsorbed CO and H was obtained by the change in partial pressure of a calibrated dosing volume in a typical chemisorption equipment, which was estimated to be ± 5% of the chemisorption value.

Table 1. Comparison of ammonia production rate over Cs-Ru/MgO and various catalysts at N₂/H₂ = 1/3 in literature at 673 K and 1.0 MPa unless otherwise stated.

Catalyst	Conditions		Catalytic Performance	
	Weight (%)	WHSV (mLg ⁻¹ h ⁻¹)	Rate (μmol metal ⁻¹ h ⁻¹)	Rate (μmol g _{cat} ⁻¹ h ⁻¹)
Cs-Ru/MgO(111)	3.7	72000	93.7	34300
	3.7	36000	66.1	24200
Cs-Ru/MgO(110)	3.5	36000	34.7	12000
Cs-Ru/MgO(100)	3.0	36000	22.9	6800
Cs-Ru/MgO(comm) ¹⁶	6.0	18000	20.6	12200
Cs-Ru/r-CeO ₂ ²⁴	4.0	18000	36.1	14300
Ru/C12A7:e ⁻²⁵	4.0	18000	15.4	6100
Fe-LiH ^{26*}	50.0	60000	1.3	11450
Ru/Pr ₂ O ₃ ¹⁶	5.0	18000	38.9	19200
Ru/Ba-Ca(NH ₂) ₂ ⁶	10.0	36000	50.4	49900
Ru/La _{0.5} Ce _{0.5} O _{1.75} ^{27**}	10.0	72000	65.7	65000

Weight % of metal loading is confirmed by ICP-MS

* Measurement done at 623K

** Measurement done at 0.9 MPa

Table 2. Summary of kinetic parameters of various Cs-promoted Ru on various MgO supports and activated carbon (AC).

Support	α (N ₂)	β (H ₂)	γ (NH ₃)
MgO(111)	+0.8	+0.6	-0.6
MgO(110)	+0.9	-0.2	-0.2
MgO(100)	+0.8	-0.5	-0.1
AC (activated carbon)	+1.2	-0.6	-0.5

¹H MAS NMR was adopted to assess the H⁺ affinity of the surface oxygen anion sites on different pure MgO supports prepared. As shown in Fig. 2a and Fig. S10, all MgO supports with residue H⁺ show two chemical shifts with one resonance at around 0.7 ppm and the other resonance at 5.43 ppm for MgO(111), 4.78 ppm for MgO(110) and 4.74 ppm for MgO(100) (see Fig. S10 for deconvoluted spectra). The first peak at around 0.7 ppm is the resonance of proton from isolated hydroxyl group (i.e. Mg-OH) and physical-adsorbed water²⁸, while second peak at lower field can be assigned to the bridging hydroxyl proton (i.e. Mg-O(H)-Mg). A significant shift from around 4.7 ppm for both nonpolar (100) and (110) surfaces to 5.4 ppm for polar (111) surface should be due to the preferential adsorption of proton induced by local electric field from surface polarity as observed in the case of ZnO²⁸.

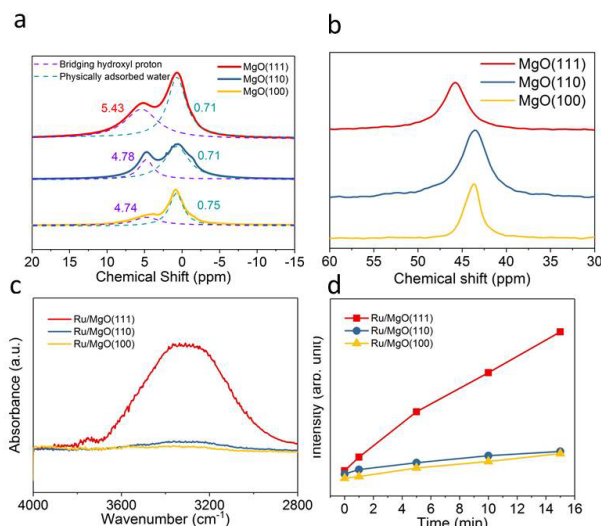


Figure 2. (a) ^1H NMR, (b) trimethylphosphine oxide (TMPO) assisted ^{31}P MAS NMR measurement of MgO(111), MgO(110), and MgO(100) supports (c) In-situ Fourier Transform IR measurement over different Ru/MgO samples after exposure of H_2 for 15 minutes (Normalised difference spectra of in-situ spectra from background spectra); (d) variation of peak intensity at 3300 cm^{-1} against time by continue flowing hydrogen gas over the Ru/MgO(111), Ru/MgO(110), and Ru/MgO(100) at 473 K .

This polarity-induced preferential proton adsorption was further confirmed by probe-assisted ^{31}P MAS NMR²⁸. The adsorption of Lewis base molecule, trimethylphosphine oxide (TMPO), is expected to interact with surface cations (i.e. Mg^{2+} or H^+) and reflect their corresponding chemical states by shifts in ^{31}P NMR. As shown in Fig. 2b, the adsorption of TMPO on bridging hydroxyl proton is indeed highly dependent on the surface polarity of the exposed MgO facet that a clear shift from 43 ppm of MgO(100) and MgO(110) to 45.8 ppm of MgO(111) can be observed (physical adsorption of TMPO at $\sim 41\text{ ppm}$). However, no interaction between TMPO and surface Mg^{2+} which is expected at higher chemical shift can be seen for three MgO supports presumably due to the easy hydroxylation nature of Mg^{2+} to Mg-OH that the interaction between this proton and TMPO is too weak to give ^{31}P chemical shift²⁰. To further ascertain the relationship between protons and the bridging O^{2-} on the polar (111) surface, in-situ Fourier Transformed IR measurement on Ru supported on the faceted MgO was carried out. Fig. 2c displays the spectra where hydrogen gas was passed onto the anhydrous Ru/MgO samples at 200°C for 15 minutes. Here the broad peak at 3300 cm^{-1} was assigned to the $-\text{OH}$ stretching region, which is stemmed from the adsorbed protons on the bridging O^{2-} . The dramatic difference in its intensity between the polar (111) facet and the other 2 facets has again shed light on the superb affinity for H and mobility of the bridging O^{2-} of this polar support phase to remove the H from Ru metal to the support surface. As displayed in Fig. S11, the peak intensity at 3300 cm^{-1} increases progressively under nitrogen, presumably due to the presence of a small degree of water in the atmosphere. Interestingly when hydrogen was passed over the sample, the intensity of which increases significantly and progressively in stark contrast compared to the other 2 facets. The density functional theory (DFT) calculations of H adsorption energy on various MgO facets were also briefly carried out and summarized in Fig. 3. It is interesting to find that the adsorption energy of H on O-terminated (111) facet (3.83 eV) is indeed more than 10 times higher than Mg-terminated (111), mixed ions-terminated (110) and (100) ($< 0.3\text{ eV}$). The Bader

charge analysis in Table S2 clearly suggests that there is a significant charge transfer from H to the electron deficient surface oxygens, resulting in the formation of surface $-\text{OH}$ groups. We attribute the large difference to the surface stabilization of intrinsically unstable polar (111) facet with dense packed partially charged oxygens on the same surface (vide infra). According to experiment (kinetic H_2 order study), characterization (IR, ^1H and ^{31}P NMR) and calculation (DFT) studies, the strong H affinity of bridging oxygen on O-terminated (111) facet that can dramatically remove strongly H poisoned Ru site for the observed enhancement in activity when polar MgO(111) is used as the support. Furthermore, as shown in Fig. S12-S14, the small difference in adsorption energy of H on atop sites and bridging sites of the O-terminated surface (0.07 eV) implies that protons can hop across the bridging oxygen sites easily. Experiment indeed shows a significantly higher H^+ conductivity over Ru-MgO(111) than other MgO facets under an applied potential, enabling high proton mobility to allow for continuous hydrogen removal from Ru active sites.

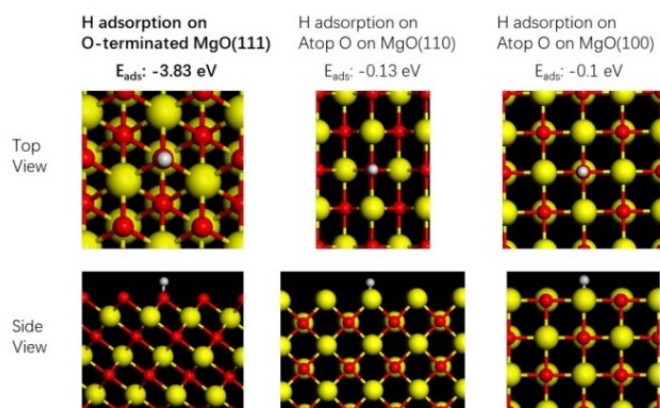


Figure 3. Schematic illustrations of molecular interaction and calculated adsorption energy from DFT between H and O atoms on various MgO surfaces: O-terminated (111), MgO(110), and MgO(100) (Mg: yellow; O: red; H: white). For MgO(111), the atoms are arranged in a layered structure which consists of pure O^{2-} layers and pure Mg^{2+} layers so that there exists both O-terminated and Mg-terminated surfaces. Meanwhile for MgO(110) and MgO(100), it is arranged in intermixed of O^{2-} and Mg^{2+} species on both the top surface and as well as the bulk, which means we can only call it as Mg site or O site in the intermix but not an entire surface. For DFT modelling, adsorption energy of H on O sites for MgO(110) or MgO(100) to O-terminated surface of MgO(111) is compared.

In order to probe the coverage as well as the extent of hydrogen spillover on the oxygen terminated surface of the polar MgO(111), operando ambient-pressure XPS at the Diamond light source (UK) was performed under dynamic switching of gases at the reaction temperature of 350°C . As seen in Figure 4 and Fig. S15-S19, the $\text{O}1\text{s}$ spectra of Ru/MgO(111) can be resolved as $[\text{OH}]$ and $[\text{O}^{2-}-\text{Mg}]$ component at approximately 531.6 eV and 529.6 eV respectively. The sample was first heated to 350°C under H_2 to remove the surface RuO_x and was then switched to Ar for the first measurement. A noticeable $[\text{OH}]$ peak was observed under Ar which was presumably due to the residual H to stabilise the unstable O^{2-} surface. It is interesting to note a significant increase in the $[\text{OH}]$ component from 13.6% to 26.3% when the gas was switched to H_2 , which could be inferred as the hydrogen spillover from Ru surface to the O^{2-} surface. This increase in surface H^+ on polar MgO(111) also agrees well with the chemisorption experiment. When the gas was subsequently switched back to Ar, the $[\text{OH}]$ component decreased correspondingly, indicating the reversibility of such phenomenon where the surface protons migrated back to the Ru. In

contrary, a broad peak was observed for Ru/MgO(111) where the line broadening was attributed to the charging effect. This also revealed the difference in the nature of conductivity of the material where charge can be channelled away in polar MgO(111) whilst retained in the non-polar MgO(110). When the gas was switched between H₂ and Ar, there was no noticeable difference between the spectra for Ru/MgO(110). In order to probe the depth and distance that the surface H⁺ can travel, depth profiling of the O1s spectra was performed at various photon energy using synchrotron XPS (Figure 4b, 4d). It is worthwhile to note the decrease of the relative [OH] signal with increasing information depth (i.e. more of the signal coming from deeper layers) is consistent with the H⁺ being located mostly near the surface, suggesting that the surface H⁺ mainly travel across the oxygen surface horizontally. In contrast, there was no noticeable change in the O1s spectra for Ru/MgO(110) in various depths, which is consistent with little or no surface H⁺ on this sample.

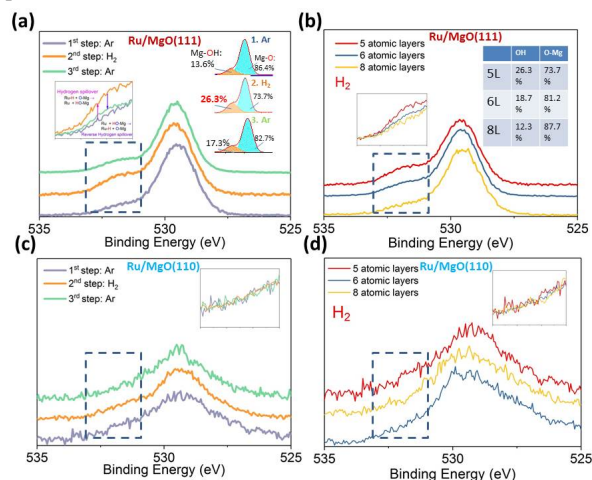


Figure 4. Operando Ambient-Pressure XPS. (a,c) O1s spectra for Ru/MgO(111) and Ru/MgO(110) respectively under consecutive switching between Ar and H₂ gas at 350 °C. Spectra were measured at a photon energy of 980 eV. (b,d) Depth profiling O1s spectra using variable photon energy under H₂ at 350 °C. “5 atomic layers” is corresponding to a penetration depth of 21.3 Å with photon energy (PE) of 980 eV; “6 atomic layers” is of a depth of 26.2 Å with PE 1280 eV; “8 atomic layers” is of a depth of 35.5 Å with PE 1880 eV. Deconvoluted O1s spectra are shown in Figure S17, S19, and S20.

Hydrogen spillover (migration) from noble metal nanoparticle to support surface in H₂ atmosphere has been previously reported²⁹. These migration has been noted over conductive or semi-conductive surfaces such as carbon and TiO₂ where electron and proton (H = H⁺ + e⁻) are both taken place in the same direction. In our case, we did not see the significant contribution to alleviate the hydrogen poisoning phenomenon for ammonia synthesis when Cs doped Ru was placed on activated carbon (Table 2). Instead, the H spillover from Ru to polar MgO (111) surface with the allergically insulating support phase is clearly observed, which appears to be a different phenomenon.

It is generally believed that the formation of ammonia from dinitrogen and dihydrogen molecules involves the formation of surface nitrogen and hydrogen adatoms on the catalyst surface. The nature of catalytic site for activation is not yet clear, however, different crystallographic sites have been suggested. For example, the B5 site of Ru hcp surface has been proposed for the activation of the

dinitrogen molecule to nitrogen atoms³⁰, while other surface ruthenium atoms may also be active for nitrogen activation³¹. It is well-accepted that there are competition between dinitrogen and dihydrogen (hydrogen poisoning) over these metal sites.^{10,12} As H atom shows stronger adsorption than N₂, the weakening or removal of H atom from this site is thus essential for the continuous production of ammonia. In our case, the employment of polar MgO(111) surface as a support for Ru with the observable polarity from our probe NMR data can offer strong electrostatic repulsion between the same oxygen anions on oxygen terminated surface, which can make the facet energetically highly unstable. Stabilization of the known polar facets can be achieved by a number of mechanisms, which include the generation of cation or anion vacancy, change in oxidation state, reconstruction of surface and adsorption of charge impurities, etc²¹. Clearly, the ionic nature of polar MgO of NaCl structure is very different from polar CeO₂³² or ZnO²⁸, the optimal Madelung stoichiometry would be prohibitively unfavorable to generate vacancy or redox alteration in Mg²⁺ cations (no strong EPR signal shown in Fig. S5) as well as surface reconstruction (see Fig. S20-S21, known to take place at > 1500°C)³³ as that of these redox oxides. As shown from our DFT calculations, the strong thermodynamic affinity of H to generate hydroxyl surface from the unstable MgO(111) with a partial charge transfer to reduce surface polarity can encourage spillover hydrogen of Ru nanoparticle at the interface. In addition, the momentarily detainment of partial negatively charge Ru can enhance back donation of electrons to activate dinitrogen, which is thought to be important to offer lower activation barrier for the ammonia production.

It is noted that a similar observation was recently made when H₂ is dissociative and reversibly activated to protons by a hydrogenase enzyme containing [FeFe] cofactor in biological system³⁴. Such that the formed electrons and protons from H₂ on the co-factor are rapidly channelled from the active enzyme: for the protons conduction, a proton-transfer pathway (PTP) using compact biological N-ligands to enhance ionization and separation of H by 1/2H₂ = H⁺ + e⁻ by Le Chatelier’s principle is identified. Thus, in our case, it is envisaged that the polar nature of close packed O²⁻ with strong electrostatic repulsion offers the energy stabilization and migration pathway for H⁺ as surface proton conductor on MgO(111) required for such H mobility on the materials’ interface with an envisaged similar role as in this existing biological system. It is exciting to correlate this surface phenomenon to the substantial enhancement of reaction rate for ammonia production alongside with biological evolution system for inspiration.

3 Conclusions:

In conclusion, we have provided experimental evidence that the hydrogen poisoning effect of Ru-based catalysts in ammonia synthesis can be alleviated by a strong local electric field using a polar MgO(111) support. The ¹H NMR, ³¹P probe-assist NMR and operando FTIR spectroscopy suggest that the preferential adsorption of proton onto the oxygen terminated surface of the polar support, which provides the driving force for adsorbed H species to migrate from the Ru surface to the O²⁻ sites and hopped as protons on the polar support under a strong local electric field. Operando AP-XPS, on the other hand, shed light on the coverage as well as the depth that the surface H⁺ can travel. Further density functional theory calculations and proton conductivity measurements reveal a small energy barrier for H⁺ to move across bridging O²⁻ sites, thus resulting in a high H⁺ mobility across the surface in contrast to MgO(110) and MgO(100). All these provide the basis for an exceptional ammonia production rate for the Ru/MgO(111) catalyst in which kinetic studies also point to a positive hydrogen removal effect. Thus, the use of MgO(111) support with the dominant polar surface

works as a more effective catalyst promotor for ammonia synthesis than that of traditional nonpolar surfaces. These findings imply the great potential factor for catalyst development in facilitating in ammonia synthesis using renewable energy at low pressure.

ASSOCIATED CONTENT

Supporting Information is included, ending with “This material is available free of charge via the Internet at <http://pubs.acs.org>.”

AUTHOR INFORMATION

Corresponding Author

edman.tsang@chem.ox.ac.uk

Notes

The authors declare no competing financial interest.

ACKNOWLEDGMENT

The financial support of this work from the EPSRC research council of UK is acknowledged. YKP acknowledges a Clarendon Scholarship for his DPhil study at the Oxford University, UK. The authors also acknowledge the use of STEM Facilities of National Institute of Advanced Industrial Science and Technology in the completion of the post-mortem studies of this work.

REFERENCES

1. Erisman, J.W., Sutton, M.A., Galloway, J., Klimont, Z., and Winiwarter, W. (2008). How a century of ammonia synthesis changed the world. *Nat. Geosci.* *1*, 636–639. Available at: <http://www.nature.com/articles/ng0325> [Accessed February 4, 2019].
2. Makepeace, J.W., Wood, T.J., Hunter, H.M.A., Jones, M.O., and David, W.I.F. (2015). Ammonia decomposition catalysis using non-stoichiometric lithium imide. *Chem. Sci.* *6*, 3805–3815. Available at: <http://xlink.rsc.org/?DOI=C5SC00205B> [Accessed February 4, 2019].
3. Klerke, A., Christensen, C.H., Nørskov, J.K., and Vegge, T. (2008). Ammonia for hydrogen storage: challenges and opportunities. *J. Mater. Chem.* *18*, 2304. Available at: <http://xlink.rsc.org/?DOI=b720020j> [Accessed February 4, 2019].
4. Kandemir, T., Schuster, M.E., Senyshyn, A., Behrens, M., and Schlögl, R. (2013). The Haber-Bosch Process Revisited: On the Real Structure and Stability of “Ammonia Iron” under Working Conditions. *Angew. Chemie Int. Ed.* *52*, 12723–12726. Available at: <http://doi.wiley.com/10.1002/anie.201305812> [Accessed February 4, 2019].
5. Bielawa, H., Hinrichsen, O., Birkner, A., and Muhler, M. (2001). The ammonia-synthesis catalyst of the next generation: Barium-promoted oxide-supported ruthenium. *Angew. Chemie - Int. Ed.* *40*, 1061–1063. Available at: <http://doi.wiley.com/10.1002/1521-3773%2820010316%2940%3A6%3C1061%3A%3AAID-ANIE10610%3E3.0.CO%3B2-B> [Accessed February 4, 2019].
6. Kitano, M., Inoue, Y., Sasase, M., Kishida, K., Kobayashi, Y., Nishiyama, K., Tada, T., Kawamura, S., Yokoyama, T., Hara, M., *et al.* (2018). Self-organized Ruthenium-Barium Core-Shell Nanoparticles on a Mesoporous Calcium Amide Matrix for Efficient Low-Temperature Ammonia Synthesis. *Angew. Chemie Int. Ed.* *57*, 2648–2652. Available at: <http://doi.wiley.com/10.1002/anie.201712398> [Accessed February 4, 2019].
7. MURATA, S. (2004). Preparation and characterization of chlorine-free ruthenium catalysts and the promoter effect in ammonia synthesis 2. A lanthanide oxide-promoted Ru/Al₂O₃ catalyst. *J. Catal.* *136*, 118–125.
8. Rosowski, F., Hornung, A., Hinrichsen, O., Herein, D., Muhler, M., and Ertl, G. (1997). Ruthenium catalysts for ammonia synthesis at high pressures: Preparation, characterization, and power-law kinetics. *Appl. Catal. A Gen.* *151*, 443–460. Available at: <https://www.sciencedirect.com/science/article/pii/S0926860X96003043?via%3Dihub> [Accessed February 4, 2019].
9. Muhler, M., Rosowski, F., Hinrichsen, O., Hornung, A., and Ertl, G. (1996). Ruthenium as catalyst for ammonia synthesis. *Stud. Surf. Sci. Catal.* *101*, 317–326. Available at: <https://www.sciencedirect.com/science/article/abs/pii/S0167299196802424> [Accessed February 4, 2019].
10. Niwa, Y., and Aika, K. (1996). The Effect of Lanthanide Oxides as a Support for Ruthenium Catalysts in Ammonia Synthesis. *J. Catal.* *162*, 138–142. Available at: <https://www.sciencedirect.com/science/article/pii/S0021951796902687?via%3Dihub> [Accessed February 4, 2019].
11. Kitano, M., Inoue, Y., Ishikawa, H., Yamagata, K., Nakao, T., Tada, T., Matsuishi, S., Yokoyama, T., Hara, M., and Hosono, H. (2016). Essential role of hydride ion in ruthenium-based ammonia synthesis catalysts. *Chem. Sci.* *7*, 4036–4043. Available at: <http://xlink.rsc.org/?DOI=C6SC00767H>.
12. Kitano, M., Inoue, Y., Yamazaki, Y., Hayashi, F., Kanbara, S., Matsuishi, S., Yokoyama, T., Kim, S.-W., Hara, M., and Hosono, H. (2012). Ammonia synthesis using a stable electride as an electron donor and reversible hydrogen store. *Nat. Chem.* *4*, 934–940. Available at: <http://www.nature.com/doi/finder/10.1038/nchem.1476>.
13. Mutch, G.A., Shulda, S., Mccue, A.J., Menart, M.J., Ciobanu, C. V., Ngo, C., Anderson, J.A., Richards, R.M., and Vega-Maza, D. (2018). Carbon Capture by Metal Oxides: Unleashing the Potential of the (111) Facet. *J. Am. Chem. Soc.* *140*, 4736–4742. Available at: <https://pubs.acs.org/sharingguidelines> [Accessed April 19, 2019].
14. Wang, F., Ta, N., and Shen, W. (2014). MgO nanosheets, nanodisks, and nanofibers for the Meerwein–Ponndorf–Verley reaction. *Appl. Catal. A Gen.* *475*, 76–81. Available at: <https://www.sciencedirect.com/science/article/pii/S0926860X14000301> [Accessed February 4, 2019].
15. Chen, J., Tian, S., Lu, J., and Xiong, Y. (2015). Catalytic performance of MgO with different exposed crystal facets towards the ozonation of 4-chlorophenol. *Appl. Catal. A Gen.* *506*, 118–125. Available at: <https://www.sciencedirect.com/science/article/pii/S0926860X15301344> [Accessed February 4, 2019].
16. Sato, K., Imamura, K., Kawano, Y., Miyahara, S. ichiro, Yamamoto, T., Matsumura, S., and Nagaoka, K. (2016). A low-crystalline ruthenium nano-layer supported on praseodymium oxide as an active catalyst for ammonia synthesis. *Chem. Sci.* *8*, 674–679. Available at: www.rsc.org/chemicalscience [Accessed April 27, 2019].
17. Bécue, T., Davis, R.J., and Garces, J.M. (1998). Effect of Cationic Promoters on the Kinetics of Ammonia Synthesis Catalyzed by Ruthenium Supported on Zeolite X. *J. Catal.* *179*, 129–137. Available at: <https://www.sciencedirect.com/science/article/pii/S0021951798922126> [Accessed February 4, 2019].
18. McClaine, B.C., Becue, T., Lock, C., and Davis, R.J. (2000). Kinetic analysis of ammonia synthesis catalyzed by barium-promoted ruthenium supported on zeolite X. *J. Mol. Catal. A Chem.* *163*, 105–116. Available at: <https://www.sciencedirect.com/science/article/pii/S1381116900004039> [Accessed February 4, 2019].
19. Zhu, K., Hu, J., Kübel, C., and Richards, R. (2006). Efficient Preparation and Catalytic Activity of MgO(111) Nanosheets. *Angew. Chemie Int. Ed.* *45*, 7277–7281. Available at: <http://doi.wiley.com/10.1002/anie.200602393> [Accessed February 4, 2019].
20. Cadigan, C.A., Corpuz, A.R., Lin, F., Caskey, C.M., Finch, K.B.H., Wang, X., and Richards, R.M. (2013). Nanoscale (111) faceted rock-salt metal oxides in catalysis. *Catal. Sci. Technol.* *3*, 900–911. Available at: <http://xlink.rsc.org/?DOI=C2CY20373A> [Accessed February 4, 2019].
21. Peng, Y.-K., and Tsang, S.C.E. (2018). Facet-dependent photocatalysis of nanosize semiconductive metal oxides and progress of their characterization. *Nano Today* *18*, 15–34.

- Available at:
<https://www.sciencedirect.com/science/article/pii/S1748013217304267> [Accessed February 4, 2019].
22. Siporin, S.E., and Davis, R.J. (2004). Use of kinetic models to explore the role of base promoters on Ru/MgO ammonia synthesis catalysts. *J. Catal.* 225, 359–368. Available at: <https://www.sciencedirect.com/science/article/pii/S0021951704001800> [Accessed February 4, 2019].
 23. Aika, K., Kumasaka, M., Oma, T., Kato, O., Matsuda, H., Watanabe, N., Yamazaki, K., Ozaki, A., and Onishi, T. (1986). Support and promoter effect of ruthenium catalyst. III. Kinetics of ammonia synthesis over various Ru catalysts. *Appl. Catal.* 28, 57–68. Available at: <https://www.sciencedirect.com/science/article/pii/S0166983400824926?via%3Dihub> [Accessed February 4, 2019].
 24. Lin, B., Liu, Y., Heng, L., Wang, X., Ni, J., Lin, J., and Jiang, L. (2018). Morphology Effect of Ceria on the Catalytic Performances of Ru/CeO₂ Catalysts for Ammonia Synthesis. *Ind. Eng. Chem. Res.* 57, 9127–9135. Available at: <https://pubs.acs.org/sharingguidelines> [Accessed April 27, 2019].
 25. Kitano, M., Inoue, Y., Yamazaki, Y., Hayashi, F., Kanbara, S., Matsuishi, S., Yokoyama, T., Kim, S.-W., Hara, M., and Hosono, H. (2012). Ammonia synthesis using a stable electride as an electron donor and reversible hydrogen store. *Nat. Chem.* 4, 934–940. Available at: <http://www.nature.com/articles/nchem.1476> [Accessed February 4, 2019].
 26. Wang, P., Chang, F., Gao, W., Guo, J., Wu, G., He, T., and Chen, P. (2016). Breaking scaling relations to achieve low-temperature ammonia synthesis through LiH-mediated nitrogen transfer and hydrogenation. *Nat. Chem.* 9, 1–7. Available at: <http://dx.doi.org/10.1038/nchem.2595> <http://www.nature.com/doi/10.1038/nchem.2595>.
 27. Ogura, Y., Sato, K., Miyahara, S., Kawano, Y., Toriyama, T., Yamamoto, T., Matsumura, S., Hosokawa, S., and Nagaoka, K. (2018). Efficient ammonia synthesis over a Ru/La_{0.5}Ce_{0.5}O_{1.75} catalyst pre-reduced at high temperature. *Chem. Sci.* 9, 2230–2237. Available at: <http://xlink.rsc.org/?DOI=C7SC05343F> [Accessed April 27, 2019].
 28. Peng, Y.-K., Ye, L., Qu, J., Zhang, L., Fu, Y., Teixeira, I.F., McPherson, I.J., He, H., and Tsang, S.C.E. (2016). Trimethylphosphine-Assisted Surface Fingerprinting of Metal Oxide Nanoparticle by ³¹P Solid-State NMR: A Zinc Oxide Case Study. *J. Am. Chem. Soc.* 138, 2225–2234. Available at: <http://pubs.acs.org/doi/10.1021/jacs.5b12080> [Accessed February 4, 2019].
 29. Karim, W., Spreafico, C., Kleibert, A., Gobrecht, J., VandeVondele, J., Ekinci, Y., and van Bokhoven, J.A. (2017). Catalyst support effects on hydrogen spillover. *Nature* 541, 68–71. Available at: <http://www.nature.com/articles/nature20782> [Accessed February 4, 2019].
 30. Logadóttir, Á., and Nørskov, J.K. (2003). Ammonia synthesis over a Ru(0001) surface studied by density functional calculations. *J. Catal.* 220, 273–279. Available at: <https://www.sciencedirect.com/science/article/pii/S0021951703001568> [Accessed February 4, 2019].
 31. Shetty, S., Jansen, A.P.J., and Van Santen, R.A. (2008). Active sites for N₂ dissociation on ruthenium. *J. Phys. Chem. C* 112, 17768–17771. Available at: <http://pubs.acs.org/doi/10.1021/jp8085478> [Accessed February 6, 2019].
 32. Herman, G.S. (1999). Characterization of surface defects on epitaxial CeO₂(001) films. *Surf. Sci.* 437, 207–214. Available at: www.elsevier.nl/locate/susc [Accessed April 25, 2019].
 33. Gajdardziska-Josifovska, M., Crozier, P.A., and Cowley, J.M. (1991). A ($\sqrt{3} \times \sqrt{3}$)R30° reconstruction on annealed (111) surfaces of MgO. *Surf. Sci. Lett.* 248, L259–L264. Available at: <https://www.sciencedirect.com/science/article/pii/016725849190336P> [Accessed February 6, 2019].
 34. Winkler, M., Senger, M., Duan, J., Esselborn, J., Wittkamp, F., Hofmann, E., Apfel, U.-P., Stripp, S.T., and Happe, T. (2017). Accumulating the hydride state in the catalytic cycle of [FeFe]-hydrogenases. *Nat. Commun.* 8, 16115. Available at: <http://www.nature.com/doi/10.1038/ncomms16115> [Accessed February 4, 2019].

Table of Contents artwork

